Journal of Asian Earth Sciences 298 (2026) 106919

Contents lists available at ScienceDirect

Journal of Asian Earth Sciences

journal homepage: www.elsevier.com/locate/jseaes

Eocene SSZ-type ophiolite from Banggi Island, Sabah (Northern Borneo), Malaysia: Zircon U-Pb ages, geochemical characteristics and tectonic implications

Rezal Rahmat [a,b,c,d], Sun-Lin Chung [b,c,e,*], Azman Abd Ghani [f], Hao-Yang Lee [b], Yoshiyuki Iizuka [b], Chih-Tung Chen [c], Long Xiang Quek [g]

[a] Taiwan International Graduate Program, Earth System Science, Academia Sinica, Taipei, Taiwan
[b] Institute of Earth Sciences, Academia Sinica, Taipei, Taiwan
[c] College of Earth Sciences, National Central University, Chungli, Taiwan
[d] Geology Program, Faculty of Science and Technology, Universiti Malaysia Sabah, Malaysia
[e] Department of Geosciences, National Taiwan University, Taipei, Taiwan
[f] Department of Geology, University of Malaya, Kuala Lumpur, Malaysia
[g] College of Earth and Planetary Sciences, University of Chinese Academy of Sciences, Beijing, China

ARTICLE INFO

Keywords:
Borneo
Sabah
Ophiolite
zircon U-Pb geochronology
Geochemistry
Subduction initiation

ABSTRACT

Ophiolites in Sabah are dispersed in a band-shaped lineament stretching from Darvel Bay in the southeast to Banggi Island in the northmost part of Sabah. This study reports the first set of zircons U-Pb ages and whole-rock geochemical data of the Banggi Island Ophiolite (BIO), conventionally regarded as part of the regional Triassic-Eocene "Chert-Spilite Formations" that had been named as the Sabah Ophiolite, and interpreted as remnants of oceanic crust from the proto-South China Sea. LA-ICPMS analyses of zircons separated from five gabbro and two diorite samples gave a short span of $^{206}Pb/^{238}U$ ages of ~ 55–50 Ma (Early Eocene), with high and positive $\varepsilon_{Hf}(t)$ values from + 16.6 to + 10.2 indicating their magma source from a relatively depleted or juvenile mantle. The crustal sequence of Banggi Island Ophiolite, including basalt, gabbro, and diorite, is characterized by depletion in the light rare earth elements and various degrees of enrichment in the large ion lithophile elements, coupled with depletion in Nb and Ta. Their overall geochemical signatures are comparable to the SSZ (supra-subduction zone)-type ophiolites reported from two nearby islands in Palawan and Mindoro, western Philippines. Integrating our new data with regional geologic information, we argue that the Banggi Island Ophiolite represents an SSZ-type ophiolite that formed in the forearc regime at the initial stage of southward subduction of the proto-South China Sea plate. The subduction initiation started from the Early Eocene in Sabah, leading to upper-plate spreading and associated magmatism that gave rise to the crustal rocks of the ophiolite. It may have caused a regional stratigraphic unconformity and later propagated eastward to Palawan and Mindoro, eventually resulting in the ophiolites there and a volcanic arc exposed now as the Cagayan Ridge.

1. Introduction

Ophiolites represent fragments of oceanic crust and underlying uppermost mantle that outcrop in orogenic belts or continental margins. Circum the South China Sea, a number of Mesozoic to early Cenozoic ophiolitic complexes are exposed from Luzon through Mindoro and Palawan to Sabah (Fig. 1a). These ophiolites, however, do not appear genetically linked to the younger South China Sea basin that is widely considered to have formed during ~ 32 to 15 Ma (Briais et al., 1993; Sibuet et al., 2016). Their generations have been attributed instead to the evolution of an older version of the modern South China Sea, i.e., the Proto-South China Sea (PSCS; Hall, 2012; Zahirovic et al., 2014), which may have been completely subducted beneath the region from North Borneo (Sabah) to Luzon-Palawan-Mindoro (Rangin et al., 1999; Hall and Spakman, 2015; Wu et al., 2016). Specifically, for example, ophiolitic rocks in northern Sabah and the western Philippines (Luzon, Mindoro, and Palawan) have been widely claimed to be the remnants of oceanic crust from the extinct Mesozoic PSCS (Hall and Breitfeld, 2017;

* Corresponding author at: Institute of Earth Sciences, Academia Sinica, Taipei, Taiwan.
E-mail address: sunlin@earth.sinica.edu.tw (S.-L. Chung).

https://doi.org/10.1016/j.jseaes.2025.106919
Received 1 September 2025; Received in revised form 11 November 2025; Accepted 18 December 2025
Available online 19 December 2025

Yumul et al., 2020; Dycoco et al., 2021). Nevertheless, the relations between these ophiolitic rocks, which should provide key information about the magmatic and tectonic history of this particular region, remain poorly explored. Despite decades of extensive mapping and petrographic studies, the formation ages and geochemical characteristics of ophiolites exposed in northern Sabah remain unclear until several recent works conducted from Kudat and Marudu Bay (Fig. 1b), suggesting that in both areas the ophiolites are of Cretaceous ages (Basir and Tongkul, 2013; Wang et al., 2023; van de Lagemaat et al., 2024). In this paper, we report for the first time a detailed study of field occurrence, petrography and whole-rock geochemistry, together with zircon U-Pb and Hf isotopic analysis of the ophiolite from Banggi Island, with which associated presence of ultramafic and mafic rocks has been documented for decades (Stephens, 1956; Wilson, 1961). Our results suggest (1) the Banggi Island Ophiolite was formed in the early Eocene, based on new zircon U-Pb ages of 55–50 Ma, (2) the magmatic rocks show LREE-depleted patterns and arc geochemical characteristics comparable to forearc magmatic rocks from the Izu-Bonin-Mariana system, (3) the Banggi Island Ophiolite, as nearby SSZ-type ophiolites from Palawan and Mindoro, can be best interpreted as relicts of a forearc crust that was formed during subduction initiation of the Proto-South China Sea plate, (4) the subduction initiation may have also led to the Eocene unconformity widespread in the northern Borneo (Sabah) region.

2. Background

2.1. The Sabah ophiolites

In Sabah, the ophiolitic association that has been traditionally called the "Chert-Spilite Formation" comprising magmatic (ultrabasic, gabbro, dolerite, and basalt), sedimentary (chert and red shale), and metamorphic (hornblende schist and gneiss) rocks, and argued to be of Triassic to Eocene ages based on radiolarian and microfossil records (Fitch, 1955; Stephens, 1956; Wilson, 1961; Newton-Smith, 1967; Leong, 1977; Basir et al., 1985). Most recently, Wang et al. (2023) have redefined the Chert-Spilite Formation as "Sabah Ophiolites". The Sabah Ophiolites (Fig. 1b) in fact have different names in locations, such as Darvel Bay Ophiolite (DBO: Omang et al., 1992; Omang, 1993), Telupid Ophiolite (TO: Chien et al., 2019), Kudat Ophiolite (KO: Omang et al., 1994), Marudu Bay Ophiolite (MBO: Rezal, 2016) and Banggi Island Ophiolite (BIO). They are now exposed and distributed in association with mélange sequences from northern to southeastern Sabah in a band-shaped lineament along a broad suture zone coined the "Kinabalu Suture" (Tjia, 1988).

As illustrated in the simplified stratigraphy (Fig. 2), the Sabah ophiolitic complexes were conventionally regarded as basement in the region (Hutchison, 1975), overlying with younger sedimentary formations deposited from the Paleogene to Neogene (Sanudin and Baba, 2007). Several sedimentary unconformities have been identified, such as the Middle Eocene one that separates the early Paleogene (Trusmadi–Sapulut Formation) and late Paleogene (Crocker–Temburung–Labang–Kudat Formation) sequences (Tongkul, 1995; Sanudin and Baba, 2007). Ophiolitic fragments and reworked nannofossils (Late Cretaceous to Early Eocene) are present in the younger Eocene formations, indicating erosion of uplifted ophiolitic complexes during the Middle Eocene (Rangin et al., 1990; Sanudin and Baba, 2007). Such unconformity is also observed in Sarawak, southwestern Sabah (Hutchison, 1996), thus having been designated as the Sarawak Orogeny Unconformity (Wang et al., 2016) or the Rajang Unconformity (Hall and Breitfeld, 2017).

An additional major stratigraphic unconformity occurred in the Miocene that separates the Paleogene and Neogene sedimentary sequences (Fig. 2). In the Early Miocene, southward drifting of rifted micro-fragments from the South China continental margin (i.e., the Dangerous Ground-Reed Bank block) started colliding with the northern Borneo-Cagayan Ridge, hence terminating subduction of the PSCS plate and resulting in a regional tectonic event referred to as the Sabah Orogeny (Hutchison, 1996). Consequently, after a sedimentary hiatus, Neogene formations were deposited largely in a shallow marine environment. From the Pliocene, the major part of North Borneo got uplifted

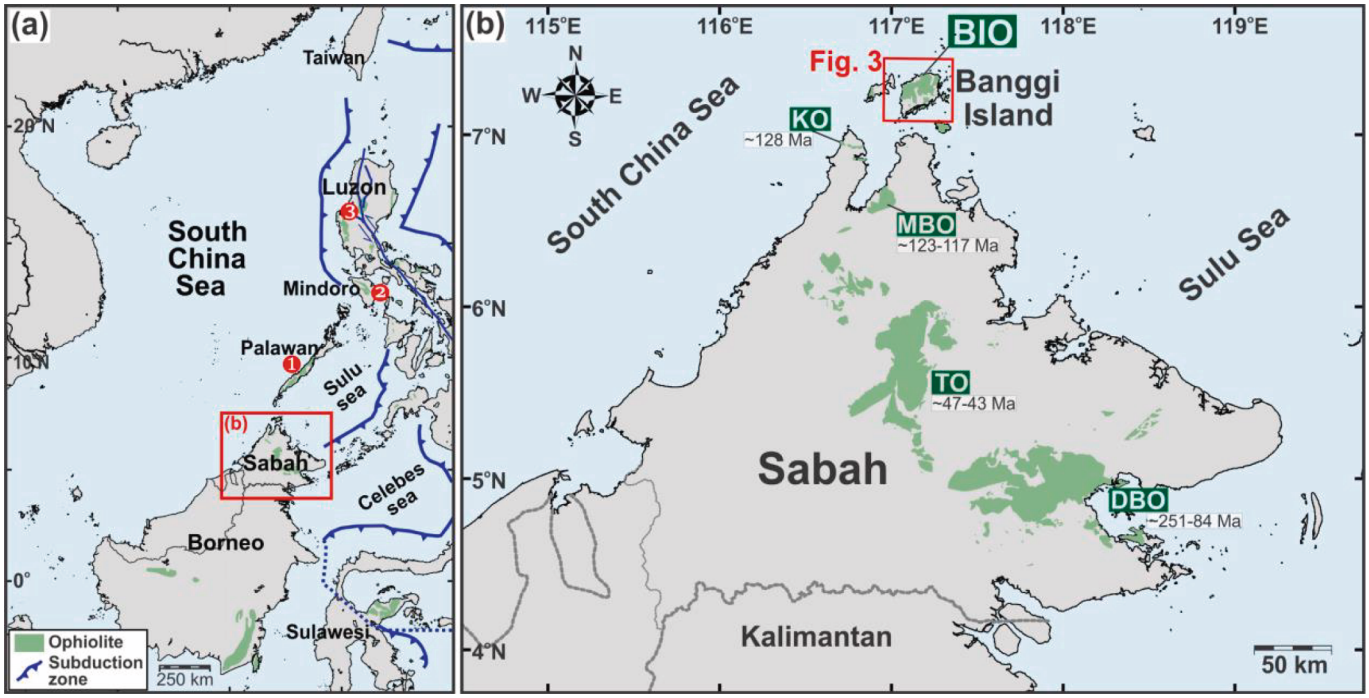

Fig. 1. (a) Simplified tectonic map of SE Asia around Sabah with distribution of ophiolites: 1. Central Palawan Ophiolite, 2. Amnay Ophiolite, Mindoro, 3. Zambales/Angat Ophiolite; (b) Outcrops of ophiolites in Sabah. BIO: Banggi Island Ophiolite, DBO: Darvel Bay Ophiolite, MBO: Marudu Bay Ophiolite, KO: Kudat Ophiolite, TO: Telupid Ophiolite. Summaries of U-Pb ages of the Sabah ophiolites (Chien et al., 2019; Burton-Johnson et al., 2020; Rezal et al., 2020, 2025; Wang et al., 2023; Tian et al., 2024; Zhou et al., 2024) are depicted.

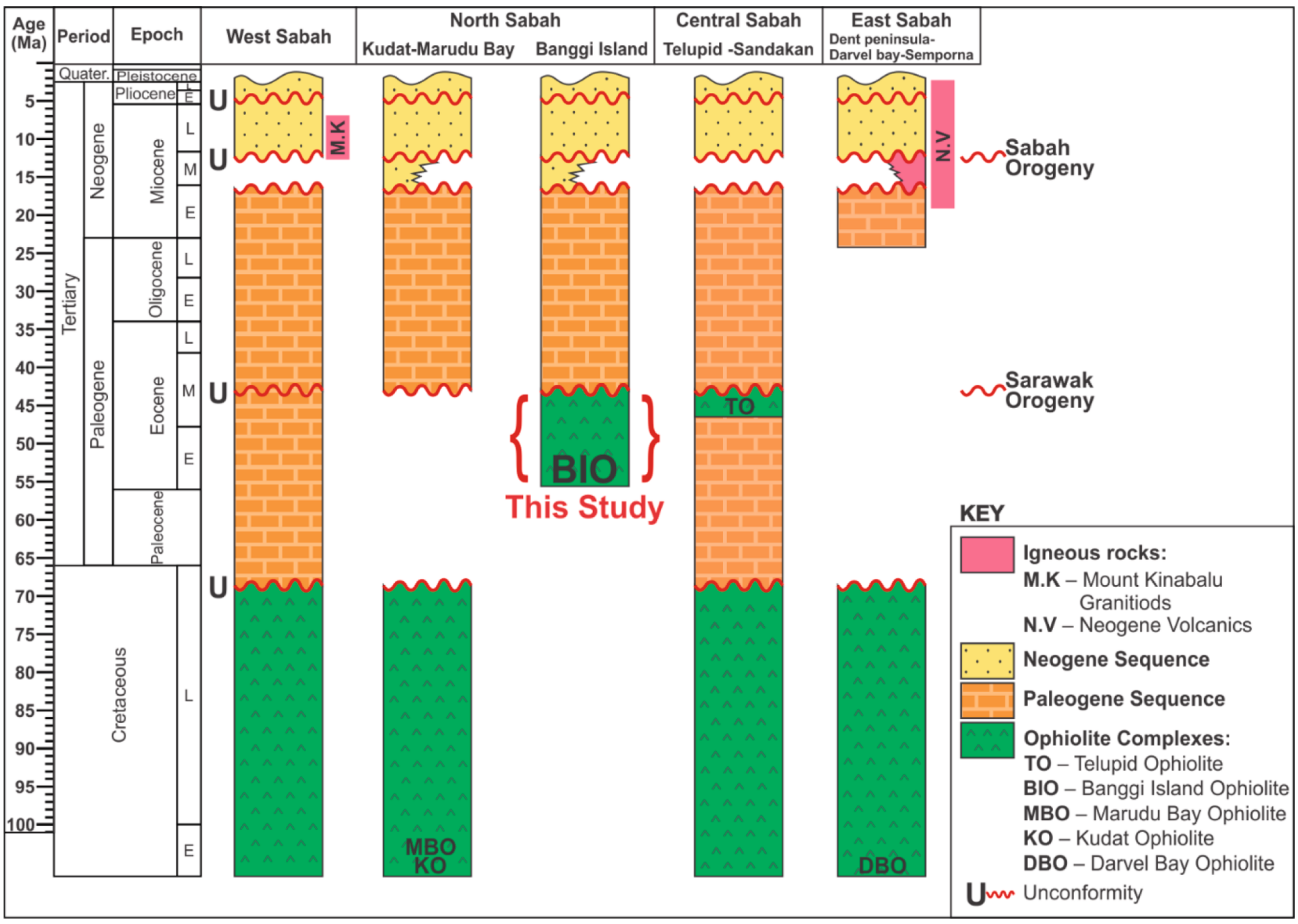

Fig. 2. Simplified stratigraphy columns of Sabah (after Sanudin and Baba, 2007; Razak, 2015).

and became a landmass due to the Sabah Orogeny (Hutchison, 1996).

2.2. Ages of the Sabah ophiolites

The ophiolite complexes in Sabah have been reported with a large age range from the Triassic to Eocene, based essentially on radiolarian and microfossil records, along with radiometric ages of the magmatic rocks. The radiolarian fossil assemblages from cherts across various locations revealed the Valanginian to the Turonian (Cretaceous) ages (Leong, 1977; Basir et al., 1985; Basir, 1992; Aitchison, 1994; Junaidi and Basir, 2012, 2013; Basir and Tongkul, 2013). Meanwhile, diverse K-Ar ages (~217–33 Ma) obtained from the magmatic rocks (Kirk, 1968; Leong, 1974; Rangin et al., 1990; Omang, 1993; Swauger et al., 1995; Omang and Barber, 1996; Graves et al., 2000) might suggest the limited accuracy of the method, potentially due to the very low K concentration of the samples (Hutchison, 2005). A recent work by Wang et al. (2023) using Ar-Ar method to date basalts sampled from different parts of the Sabah Ophiolite, including KO, MBO, TO and DBO, also gave a wide range of ages from ~ 184 to 92 Ma, despite broadly coinciding with the existing K-Ar dates.

More recently, zircon U-Pb ages from different locations have been reported. The oldest ones, dated at 251 Ma and 241 Ma, were obtained from arc-type granitoid rocks in the Segama Valley of the DBO (Burton-Johnson et al., 2020). In DBO area, studies have identified LREE-depleted gabbros that contain ~ 210–230 Ma magmatic zircons (Chien et al., 2019) and LREE-enriched gabbro-diabase with zircon U-Pb ages at ~ 231–245 Ma (Tian et al., 2024; Zhao et al., 2024). Two gabbros from the KO and the MBO, respectively, yield Early Cretaceous ages of ~ 128 Ma and ~ 122 Ma (Rezal et al., 2020). In contrast, apparently younger Eocene zircon U-Pb ages (~46–43 Ma) were obtained from gabbro samples from the TO (Chien et al., 2019), which are different from Tsikouras et al. (2021) reporting zircon U-Pb ages as young as middle Miocene (9.2–10.4 Ma) for ophiolitic rocks from Ranau and Telupid in the same area. However, Cullen and Burton-Johnson (2021) commented that these Miocene zircons are metasomatic or related to the nearby Miocene magmatism in Mount Kinabalu.

2.3. The Banggi Island Ophiolite (BIO)

Banggi Island situates off northern Sabah (Borneo) and ~ 100 km in the south of Palawan, Philippines (Fig. 1). This region is adjacent to three marginal seas, namely, the South China Sea, the Sulu Sea, and the Celebes Sea (Fig. 1a). Main geological units on Banggi Island are the ophiolite complex and sedimentary sequences, including Crocker Formation, South Banggi Formation, Bongaya Formation and Alluvium (Fig. 3a). The ophiolite complex, presumably of Cretaceous to Paleogene ages (Wilson, 1961), consists of diverse rock types from ultrabasic to acidic magmatic rocks, together with chert-shale interbeds. Such ophiolitic basement rocks are overlain by younger sedimentary formations of Paleogene to Neogene ages (Fig. 2). The late Paleogene formation is the Crocker Formation, exposed as several minor sections of turbidite. The Neogene sedimentary rocks are more abundant and represented by the Bongaya Formation and the South Banggi Formation (Fig. 3a). Despite decades of field mapping studies (Stephens, 1956; Wilson, 1961), more detailed analyses of the BIO are lacking and thus its formation age remains uncertain.

3. Field and petrography observation

Field occurrence of the ophiolitic rocks in northern Sabah (including

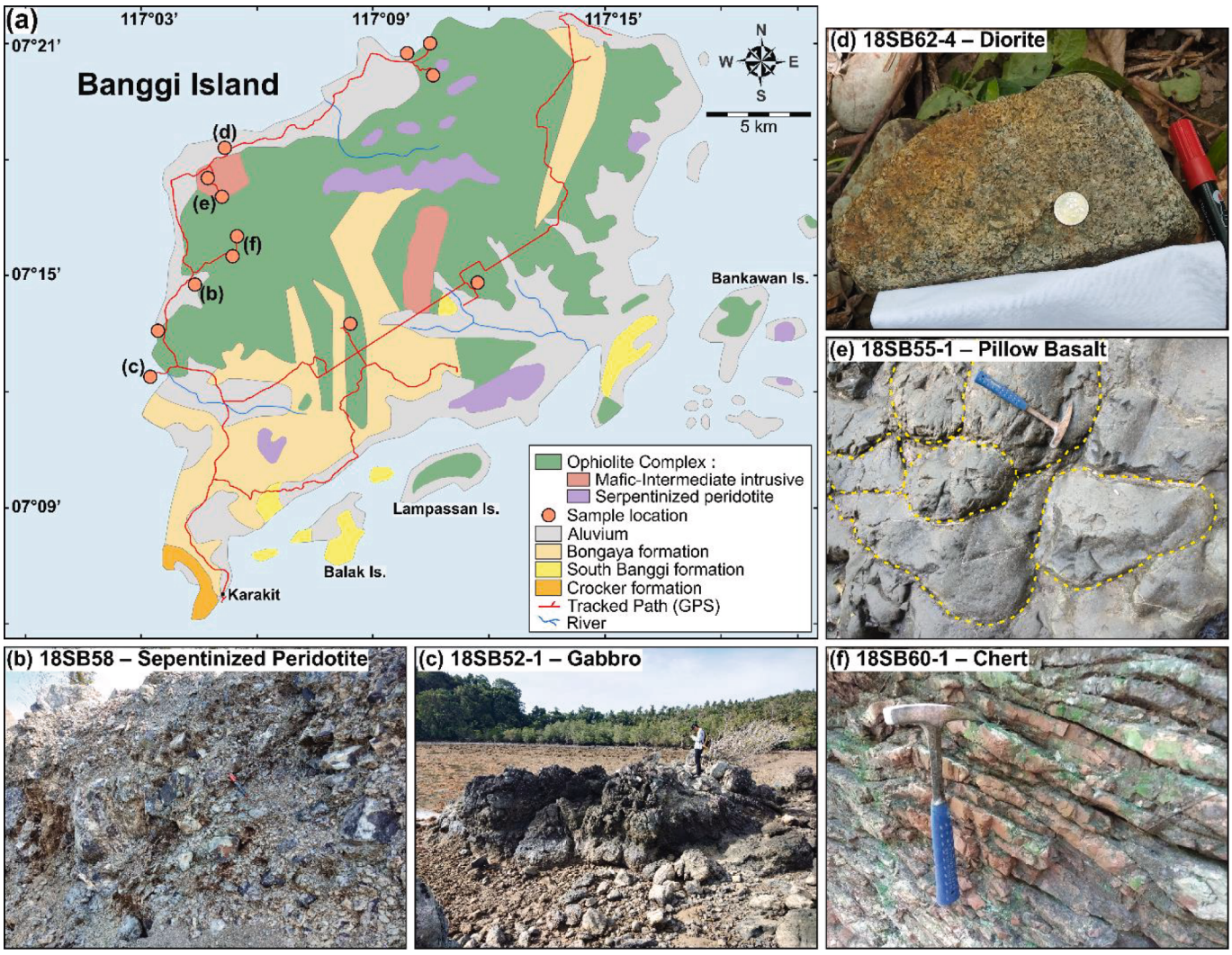

Fig. 3. (a) Simplified geological map of Banggi Island (after Razak, 2015); and selected outcrop photographs of (b) fractured serpentinized peridotite, (c) gabbro in coastal area during low tide, (d) diorite boulder, (e) basaltic pillow lava, and (f) layered red ribbon chert.

Banggi Island) has been documented since Stephens (1956) and Wilson (1961). The BIO consists of ultramafic to intermediate igneous rocks and chert, in association with metamorphic rocks and chromite deposits. Despite their discontinuous occurrences, these rock types closely correspond to the key components of a classical ophiolite sequence described by the Penrose Conference (Anonymous, 1972), suggesting they may constitute a dismembered ophiolitic complex. Based on field and petrographic observations, we divide it into five main rock units: ultramafic, gabbroic, felsic plutonic (granitoid), volcanic, and deep-sea sedimentary rocks, with the field photos of major rock types and sample localities shown in Fig. 3 and additional information given in Supplementary Table S1.

3.1. Ultramafic unit

Ultramafic rocks, obtained from outcrops and river boulders, are dark blue-green or black (Fig. 3b). The rocks are mainly of harzburgitic composition, with MgO = 40–38 wt% (Wilson, 1961), and predominantly serpentinized to varying degrees, associated with joints or fractures filled by secondary green serpentine and white talc. Slickenside features are observed in every outcrop. Under microscopic view (Fig. 4a), almost all primary minerals are altered and replaced by serpentines. The serpentinization occurs with fibrous replacement, filling cracks and crystal boundaries, thus producing a typical mesh texture. In occasion, the relic of original minerals, such as olivine preserved its rounded and high relief feature while pyroxene kept its cleavages, can still be observed. Opaque chrome-spinel is present in some samples.

3.2. Gabbroic unit

A small gabbroic rock outcrop (approximately ~ 20 m) is exposed in the coastal region of Banggi Island, but it is only accessible during low tides (Fig. 3c). In addition to this limited outcrop, there are plenty of gabbroic boulders at upstream areas with sizes ranging from several centimetres up to 2–5 m. The gabbroic rocks are medium- to coarse-grained and appear dark grey to green in colour. No clear foliation, lineation, or layering features are observed on these gabbroic rocks.

Petrographic observation of the gabbroic samples (18SB52-1, 18SB52-2, 18SB62-2, and 18SB67-2) suggests a cumulate feature. These samples are coarse-grained (up to 1 mm) and mostly contain pyroxene + plagioclase ± olivine. Pyroxenes are colourless to light brownish crystals that appear subhedral, tabular, or prismatic in shape. These pyroxenes may exhibit crystal twinning and show replacement by green chlorites, possibly from alteration. Poikilitic and ophitic features are common, with idiomorphic clinopyroxene enclosing several tiny laths of plagioclase crystals (Fig. 4b). Plagioclases exhibit traces of alteration resulting in a turbid surface with unclear twinning. Noticeable amounts of Fe-Ti oxide are present in some gabbro samples.

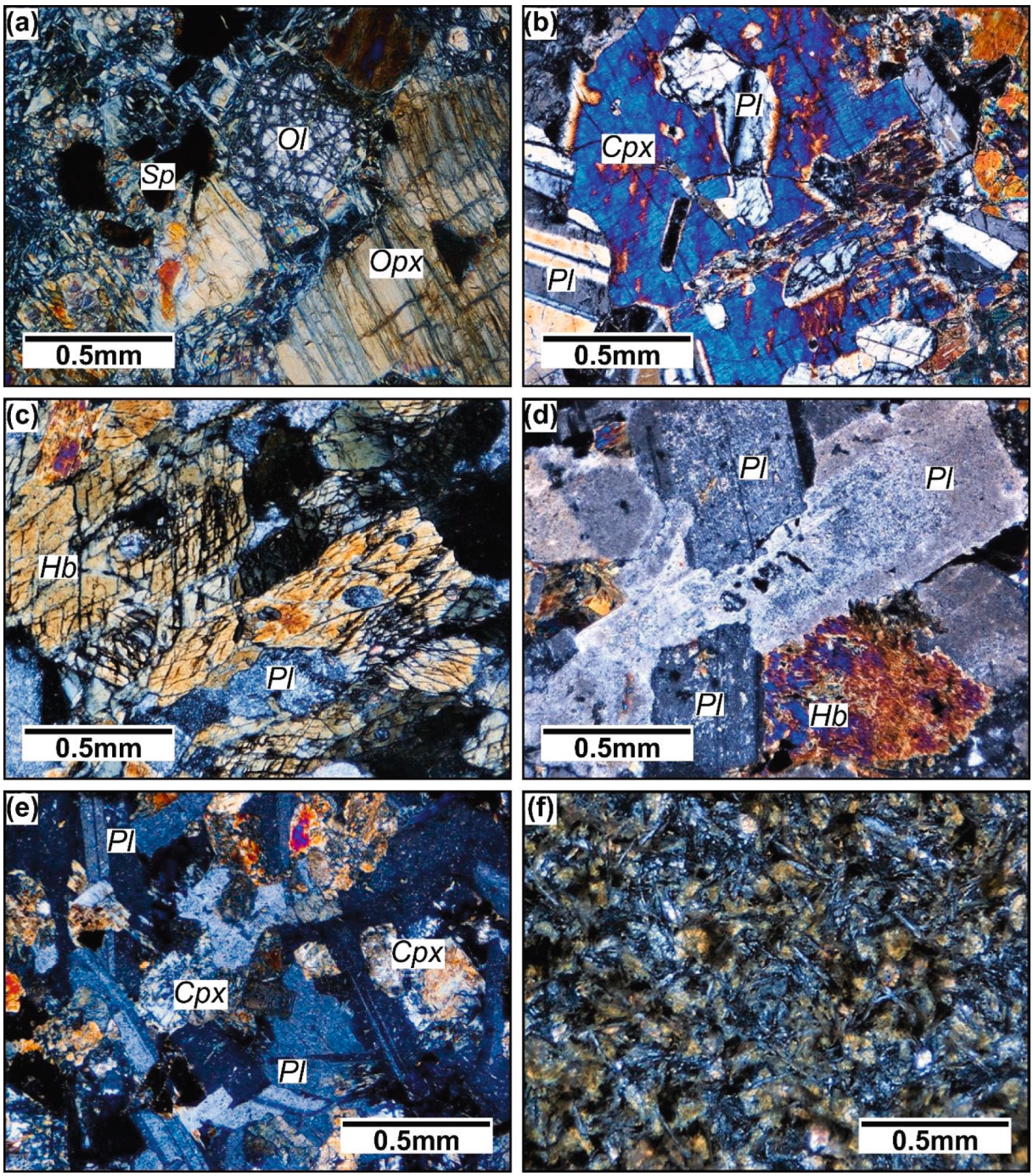

Fig. 4. Photographs (crossed-nicols) of selected samples from the Banggi Island Ophiolite: (a) 18SB58 serpentinized peridotite, (b) 18SB52-1 gabbro, (c) 18SB59-3 Hb gabbro, (d) 18SB60-3 diorite, (e) 18SB59-2 basalt/dolerite and (f) 18SB55-1 pillow basalt. (Ol = olivine; Opx = orthopyroxene; Cpx = clinopyroxene; Sp=Spinel; Hb = hornblende; Pl = plagioclase).

Hornblende gabbros (18SB44-2, 18SB44-3, 18SB54-2, 18SB59-3, and 18SB56) are also observed and have medium- to coarse-grained hypidiomorphic crystals that consist mainly of plagioclase, hornblende and pyroxene, with minor amounts of quartz and accessory minerals such as zircon and apatite. Subhedral to euhedral hornblende is green to brown, displaying a typical 120^{O} cleavage, and usually appears inclosing plagioclase in poikilitic texture (Fig. 4c). Plagioclase is mostly altered to sericite, calcite, and epidote, resulting in turbid crystal surfaces and unclear twinning. In sample 18SB59-3, a significant amount of tiny zircon appears to be embedded in the hornblende. Brecciated features are present in most samples, implying brittle deformation after crystallization.

3.3. Felsic plutonic rocks (Granitoid)

Occurrence of light-coloured plutonic rocks (diorite, quartz diorite, tonalite and trondhjemite) is common in ophiolite complexes worldwide (e.g., Oman: Rollinson, 2009; Troodos: Chen et al., 2020). In Banggi Island, there are limited amounts of felsic plutonic rocks marked on the geological map (Fig. 3a), as reported by Wilson (1961). Larger boulders of diorite rocks (Fig. 3d) appear upstream of the river, ranging in size from 20 cm to blocks of > 1 m. Four samples (18SB60-3, 18SB60-4,

18SB62-4 and 18SB62-6) were collected and have a similar mineralogy consisting of plagioclase, K-feldspar, quartz and hornblende. The feldspars reveal euhedral to subhedral, prismatic or tabular shapes, with some degree of alteration to sericite causing turbid crystal surface and lack of twinning (Fig. 4d). Exsolution between quartz and feldspar can be observed, producing a graphic texture. The main mafic mineral is hornblende, which occurs as euhedral to subhedral crystal occasionally with twinning.

3.4. Volcanic unit

Pillow basalt is the most abundant magmatic rock outcropped in western and northern coastal areas and exposed further upstream at the Bungga waterfall (Fig. 3e). It occurs as very fine- to fine-grained rocks and usually dark-greyish in colour. They show rounded, elliptical or tubular-shaped pillow structures with distinctive radial cooling joints (formed during the rapid cooling process). The pillows vary in sizes, ranging from ~ 10 to 60 cm, and sometimes can reach more than ~ 1 m in diameter. Amygdaloidal or vesicular features are well preserved, commonly with calcite veins. No clear basaltic dyke or sheeted dyke complex was found, but basaltic (doleritic) boulders with large plagioclase phenocrysts (~5 to > 10 mm) is present in river upstream.

Most aphanitic pillow basalts consist of plagioclase + pyroxene + volcanic glass ± olivine and Fe-Ti oxide arranged in an intersertal texture. The plagioclase lath is subhedral, elongated and prismatic, showing turbid surface and blurry twinning due to chlorite and sericite alteration (Fig. 4f). Plagioclase in some medium-grained basalt (dolerite) occurs as phenocrysts (~0.5 to > 2 mm) with albite twinning. Euhedral to subhedral clinopyroxene appear as phenocrysts and oikocrysts, inclosing plagioclase in a poikilitic texture (Fig. 4e). Olivine is rare and, if present, replaced by serpentine or iddingsite. Glomerophyric texture consisting of clustered phenocrysts of plagioclase and pyroxene can be observed in some samples.

3.5. Deep-sea sediments

Marine sediments that represent the uppermost sequence of the ophiolite complex occur as red ribbon chert. The chert is outcropped as thin layers (~2 to 10 cm) in several cut slopes and rivers upstream (Fig. 3f). In places, the chert shows complex faulting and folding structure, indicating subsequent deformation.

4. Analytical methods

4.1. Zircon u-pb dating analysis

Zircon grains were separated by conventional methods combining heavy liquid and magnetic separation techniques. Zircon separates, then, were handpicked under a binocular microscope, mounted in epoxy resin and polished before transmitted and reflected light images were taken under an optical microscope. Cathodoluminescence (CL) images were taken for examining the internal structures (zoning and inclusions) of individual grains and selecting the suitable spot for subsequent analyses.

The zircon U-Pb isotopic analyses were measured at the Institute of Earth Sciences, Academia Sinica using a quadrupole Agilent 7900 Q-ICP-MS equipped with a Photon Machines Analyte G2 laser ablation system (Photon Machines, Inc., Redmond, USA) that utilizes a 193 nm ArF Excimer laser with a 5 ns pulse duration. All analyses were done using a spot diameter of 35 μm with the laser repetition rate of 5 Hz, energy output of 55 %, and beam density of 5.75 J/cm^2. GJ-1 zircon (Jackson et al., 2004) was used as the primary standard for calibration. Two other zircon reference materials 91,500 and Plešovice gave weighted mean ages of 1073.1 ± 9.9 (2σ, n = 22) and 334.9 ± 3.2 (2σ, n = 18), respectively, consistent with their recommended values. The GLITTER (https://www.es.mq.edu.au/gemoc/glitter) software package was utilized for U-Th-Pb isotope data reduction and raw calculations. The common lead was corrected following the method by Andersen (2002). The weighted mean U-Pb ages and concordia diagrams were constructed using ISOPLOT software version 4.15. More detailed zircon U–Pb analytical procedures refer to Chiu et al. (2013).

4.2. Zircon Hf-isotope analysis

In-situ zircon Hf isotope analysis was conducted on the dated spot or nearby areas using a Nu Plasma HR multi-collector (MC) ICPMS attached to a Photon Machines Analyte G2 laser ablation system, equipped at the same institute. Each zircon grain takes ~ 2 min to analyse, including 30 s of the background noise check and ~ 85 s of the sample intensity after laser ablation. The measurement was set up with a beam size of 50 μm, 5–8 Hz repetition rate, and an energy of ~ 8 to 9 J/cm^2. Helium gas of ~ 0.9 L/min (MFC1 = ~0.7 L/min and MFC2 = ~0.2 L/min) was used as a carrier that transported the ablated sample from the laser-ablation section through a mixing chamber, where it was mixed with Ar gas of ~ 0.8 L/min prior to entering the ICP torch. The helium carrier gas can substantially reduce the deposition of ablated material onto the sample surface and greatly improve transport efficiency, thus increasing the signal intensity. Mud Tank zircon standard, yielding a mean $^{176}Hf/^{177}Hf$ ratio of 0.28249 ± 0.00002 (n = 22) throughout the analyses of this study, was used as the primary reference material to monitor the analytical condition of reproducibility and accuracy. Analytical isotopic ratios of $^{176}Yb/^{177}Hf$, $^{176}Lu/^{177}Hf$ and $^{176}Hf/^{177}Hf$ are reported with 2σ error. Each dated zircon grain was analysed for Lu-Hf isotopic ratios at the same spot where the U-Pb age was obtained. To ensure the data reliability, we avoided zircons with $^{176}Yb/^{177}Hf > 0.1$ (too high for precisely correcting isobaric interference of ^{176}Yb on ^{176}Hf). The Lu–Hf isotope results are listed in Supplementary Table S3.

4.3. Whole-rock geochemical analyses

Fresh portions of selected samples were used for whole-rock major and trace element analyses. They were broken and cut into small chips, crushed by a jaw crusher and ground in an agate ball mill, yielding sample powders suitable for geochemical analyses. Major element concentration was determined using glass-beads by X-ray fluorescence spectrometry (Rigaku® RIX 2000) at the Department of Geoscience, National Taiwan University, with analytical uncertainties generally better than 5 % for all elements. Trace element concentrations were obtained by dissolving the glass beads in Teflon beakers using HF + HNO3 acid mixture, then analyzed using Agilent® 7500cx Q-ICP-MS at the Institute of Earth Science, Academia Sinica, Taiwan.

5. Results

5.1. Zircon u-pb ages

To constrain the formation age of the BIO, a total of seven magmatic samples, including three gabbros, two hornblende gabbros and two diorites, all of which possess abundant zircon separates were subjected to zircon U-Pb age determination (Fig. 5). Detailed analytical results are listed in Supplementary Table S2.

Zircon separates from gabbro sample 18SB52-1 (Fig. 5a) are subhedral to anhedral, with sizes from 50 to 200 μm in elongated shape (1:1–4:1 length-to-width ratio). They reveal a large range in Th (68 to 2673 ppm, average of 994 ppm) and U (107 to 1050 ppm, average of 436 ppm) concentrations, but yield consistent $^{206}Pb/^{238}U$ ages from ~ 60 to 54 Ma, with a weighted mean of 55.4 ± 0.5 Ma (2σ, MSWD = 0.91, n = 19), constraining the crystallization age of the host magma.

Zircons from gabbro sample 18SB67-2 are subhedral to anhedral, mostly with prismatic and elongated shape (2:1–4:1 length-to-width ratio) and sizes from ~ 50–210 μm. Their CL images exhibit partly

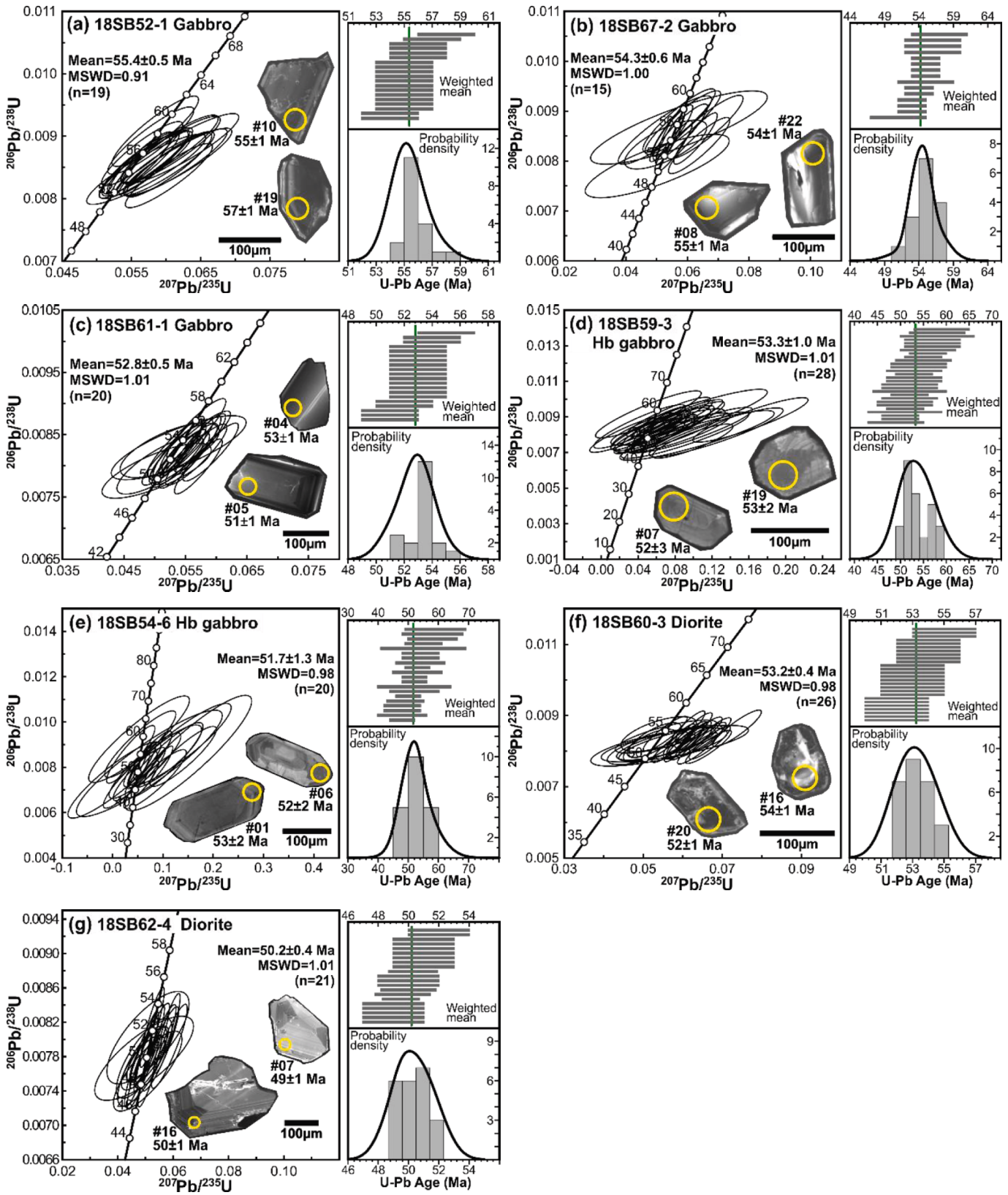

Fig. 5. Zircon U-Pb Concordia diagrams of (a) gabbro 18SB52-1, (b) gabbro 18SB67-2, (c) gabbro 18SB61-1, (d) Hb gabbro 18SB59-3, (e) metagabbro 18SB54-6, (f) diorite 18SB60-3, and (g) diorite 18SB62-4.

developed crystal faces resembling broken fragments, especially smaller grains. They have highly variable Th (6 to 4868 ppm) and U (3 to 1258 ppm) concentrations, mostly with low U contents (average of 378 ppm), which led to poor precision in individual analyses. Concordant plots yield a weighted mean $^{206}Pb/^{238}U$ age of 54.3 ± 0.6 Ma (2σ, MSWD = 1.0, n = 15; Fig. 5b), interpreted as the crystallization age of the sample.

Zircons from the third gabbro 18SB61-1 are subhedral to anhedral, with sizes from 70 to 150 μm (2:1–4:1 length-to-width ratio). Larger grains are generally prismatic and elongated, while smaller grains show broken fragments and partly developed crystal faces, as commonly observed in zircons from mafic magmas. CL images are characterized by oscillatory zoning often with a darker core. Despite their variable Th (221–5156 ppm) and U (370–2836 ppm) concentrations, these zircons yield rather homogeneous U-Pb isotopic ratios and a weighted mean $^{206}Pb/^{238}U$ age of 52.8 ± 0.5 Ma (2σ, MSWD = 1.01, n = 20; Fig. 5c).

Zircons from a hornblende gabbro (18SB59-3) are euhedral to subhedral and size from 50 to 150 μm, with most of the grains < 100 μm showing stubby and sub-rounded shapes. These zircons have low concentrations of Th (1–89 ppm) and U (11–48 ppm), averages of 6 and 22 ppm, respectively. Most of them yield inferred U-Pb ages between ~ 62–46 Ma, except for two grains (18SB59-3–21 and 18SB59-3–14) showing older ages of 96 ± 4 Ma and 70 ± 5 Ma (Table S2). The Eocene magmatic zircons gave a weighted mean $^{206}Pb/^{238}U$ age of 53.3 ± 1.0 Ma (2σ, MSWD = 1.01, n = 28; Fig. 5d).

Zircons from another hornblende gabbro 18SB54-6 are euhedral to subhedral with sizes from 50 to 200 μm. Most of the zircons occur as stubby and sub-rounded crystals with prismatic and elongated shapes (length-to-width ratio of 2:1–4:1). They have very low concentrations of U (1–48 ppm) and Th (0.01–12 ppm), with averages of ~ 15 and ~ 1 ppm, respectively. Their inferred U-Pb ages range from ~ 63–45 Ma except for two grains (18SB54-6–10 and 18SB54-6–32), dated at 117 ± 21 and 82 ± 20 Ma, respectively (Table S2). The magmatic zircons yield a weighted mean $^{206}Pb/^{238}U$ age of 51.7 ± 1.3 Ma (2σ, MSWD = 0.98, n = 20; Fig. 5e).

Zircons from a diorite sample 18SB60-3 are subhedral to anhedral crystals < 100 μm in size (~50 to 90 μm) and often appear in stubby and sub-rounded-shapes. The larger grains are mainly prismatic and elongated crystals with a 2:1 length-to-width ratio. Cathodoluminescence (CL) images show somewhat turbid surface and often oscillatory zoning. They also have a wide concentration range of U (226–3250 ppm) and Th (48–4492 ppm), averages of 1025 and 1560 ppm, respectively. The magmatic zircons yield a confined age range from ~ 50 to 59 Ma, with a weighted mean $^{206}Pb/^{238}U$ age of 53.2 ± 0.4 Ma (2σ, MSWD = 0.98, n = 26; Fig. 5f).

Zircons from another diorite 18SB62-4 are subhedral to anhedral crystals with sizes from 80 to 300 μm and length-to-width ratios of 2:1–4:1. Most larger grains have prismatic shapes, while the smaller grains appear as broken fragments exhibiting partly developed crystal faces. Cathodoluminescence (CL) images reveal turbid surface and oscillatory zoning in larger grains. These zircons show variable U (78–852 ppm) and Th (29–2790 ppm), with averages of 385 and 598, respectively. They yield U-Pb ages from ~ 48 to 55 Ma, with a mean age of 50.2 ± 0.4 Ma (2σ, MSWD = 1.01, n = 21; Fig. 5g).

5.2. Zircon Hf isotopes

A total of 44 selected zircon grains that match the data reliability test ($^{176}Yb/^{177}Hf < 0.1$) are reported in this study. They are mostly from the two hornblende gabbros, 18SB54-6 (n = 18) and 18SB59-3 (n = 20). The other dated samples, i.e., three gabbros and two diorites, contain only few zircons, 18SB60-3 (n = 4), 18SB61-1 (n = 1) and 18SB62-4 (n = 1), qualified for precise $^{176}Hf/^{177}Hf$ isotopic measurement (Table S3). Even so, they all together yield a narrow range of initial $^{176}Hf/^{177}Hf$ ratios from 0.28322 to 0.28304. These ratios correspond to high positive εHf(t) values from + 16.6 to + 10.2 (average= +13.6), plotted along or close to the Hf isotopic evolution line of the depleted mantle (Fig. 6), suggesting the magma derivation from a depleted or juvenile mantle source. Note that the high and positive Hf isotopic values of the BIO zircons are comparable to those of younger detrital zircons from Luzon, Philippines (Fig. 6), composed essentially of a juvenile oceanic arc system (Tsai

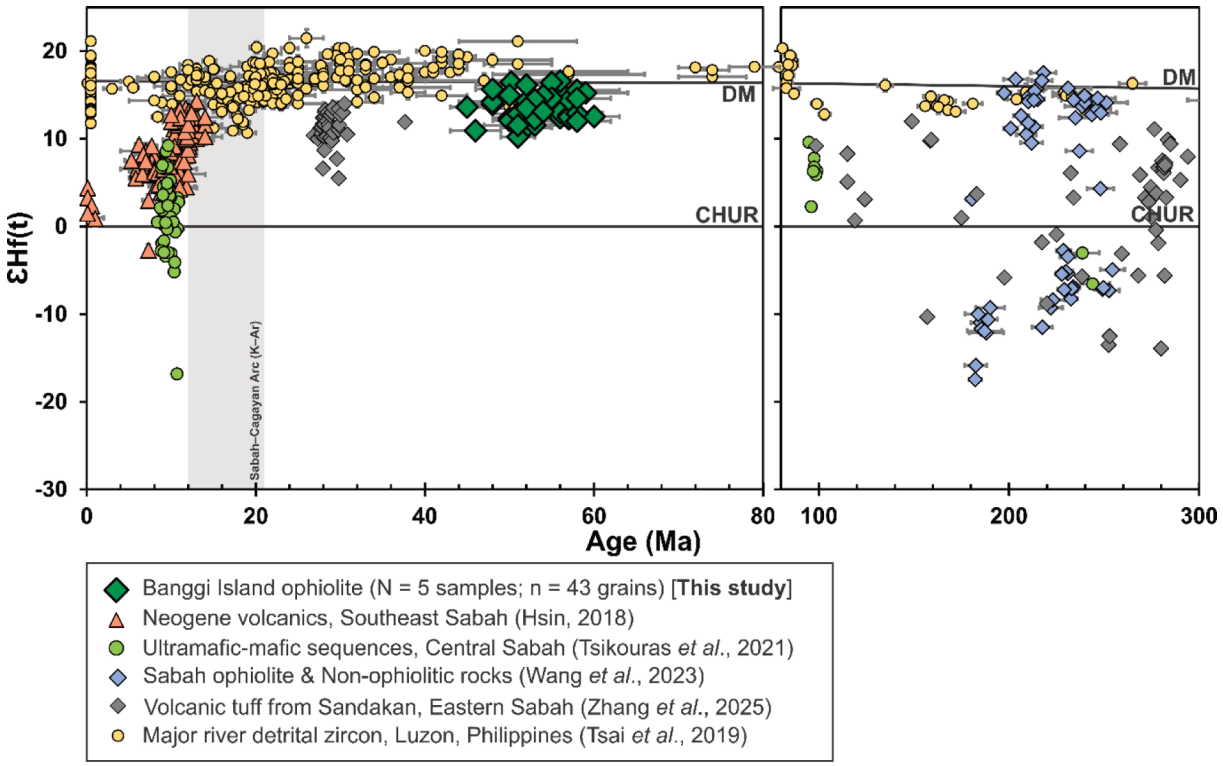

Fig. 6. Zircon U-Pb age vs. $\varepsilon_{Hf}(t)$ diagram of the Banggi Island Ophiolite, plotted with relevant zircon data from Sabah and Philippines.

et al., 2019). In contrast, the mid-Miocene zircons from the TO reported by Tsikouras et al. (2021) show apparently lower or even negative εHf(t) values (Fig. 6), overlapping with magmatic zircons from the Miocene volcanic rocks from Southeast Sabah (Zhang et al., 2025) and from the nearby Kinabalu granites (Hsin, 2018), and thus lending support to Cullen and Burton-Johnson (2021)'s viewpoint that, however, is beyond the scope here and will be discussed elsewhere in a separate article.

5.3. Whole-rock geochemistry

Thirty-four samples were analysed for whole-rock major elements and nineteen of them were analysed for trace element compositions (Supplementary Table S4).

Most BIO samples experience traces of alteration as observed petrographically and from their LOI contents (Table S4). The rocks show wide SiO_2 contents ranging from 44 to 63 wt%, portraying a composition variation from basaltic to andesitic/dioritic (Fig. 7). They comprise a subalkaline trend (Fig. 7a), except for few samples that show somewhat deviated alkali contents owing probably to alteration effect on certain mobile elements. Their TiO_2 and MgO contents vary significantly of 0.14–2.9 wt% and 0.9–16 wt%, respectively (Table S4), with the gabbros showing the lowest TiO_2 (0.14–0.25 wt%) and rather high MgO (9.3–11.8 wt%).

The basalts and hornblende gabbros are characterized by apparent depletion in the light rare earth elements (LREE) in the chondrite-normalized diagram (Fig. 8; a and c), resembling that of the normal mid-ocean ridge basalt (N-MORB). In the multi-element diagram, relative to N-MORB (Fig. 8; b and d), these mafic samples generally show enrichments in the large ion lithophile elements (LILE; e.g., Rb and Ba) and variable depletions in the high field strength elements (HFSE; Nb and Ta). Overall, their distribution pattern is comparable to that of forearc basalts from the Izu-Bonin-Mariana subduction system (Fig. 8; a-d), as well as mafic rocks of other Cenozoic SSZ-type ophiolites from adjacent regions (e.g., Central Palawan and Amnay, Mindoro; Fig. 8).

The three gabbros analyzed exhibit significantly lower REE abundance (Fig. 8c), with general features mimicking to that of fore-arc cumulate gabbros from the Izu-Bonin-Mariana system (Fig. 8; c-d). Along with the positive spikes of Eu, Ba and Sr, reflective of plagioclase accumulation, noticeable Zr-Hf depletion is observed in two samples (Fig. 8d). HFSE depletion appears also in these gabbros (Fig. 8d) and more evolved diorites (Fig. 8f). The diorites plot into two subgroups (Fig. 8e), comparable respectively to forearc and protoarc magmatic rocks from the Izu-Bonin-Mariana system (Fig. 8; e and f).

6. Discussion

6.1. Discovery of an Early Eocene ophiolite

This study produces the first precise zircon U-Pb ages for seven samples from the Banggi Island Ophiolite. The analysed zircons are typically euhedral to subhedral and prismatic crystals of sizes ~ 50–300 μm in length. These zircons are mostly concordant and yield $^{206}Pb/^{238}U$ weighted mean ages from 50.2 ± 0.4 to 55.4 ± 0.5 Ma (Fig. 5), representing their crystallization ages from host magmas. This Early Eocene formation age (~55–50 Ma) of the BIO magmatic rocks (gabbros to diorites) is apparently younger than most of the radiometric (K-Ar, Ar-Ar and U-Pb) ages reported from northern Sabah, but broadly contemporaneous and comparable to the U-Pb zircon ages from several neighbouring ophiolites such as the Telupid ophiolite, central Sabah (~46–42 Ma; Chien et al., 2019). Moreover, in nearby islands, slightly younger ophiolite complexes have been documented from Zambales, western Luzon (~48–42 Ma; Encarnacion et al., 1993; Yumul et al., 2020), Central Palawan (~40–34 Ma; Keenan et al., 2016; Dycoco et al., 2021) and Amnay, Mindoro (~33–23 Ma; Yu et al., 2020), suggesting a widespread tectonic or petrogenetic correlation (see below for discussion).

6.2. Geochemical systematics of the BIO

Considering the alteration effect, in this section we choose only immobile elements for geochemical fingerprinting analysis. Despite the BIO magmatic rocks mostly show N-MORB-like REE patterns and relative depletion in the HFSE (Fig. 8), only those with overall patterns similar to the BIO basalts should be taken into account for the geochemical correlation because the discrimination diagrams (Fig. 9) are designed primarily using volcanic rocks. The gabbros, showing apparently lower REE abundance (Fig. 8c) indicative of a cumulate origin, should be excluded. The Nb/Yb ratios of the BIO magmatic rocks, however, range between 0.18 and 1.05 (average = 0.62), similar to the N-MORB value (Nb/Yb = 0.76; Sun and McDonough, 1989), clearly indicating a depleted mantle source. This is consistent with zircon Hf isotopic data (Fig. 6), which suggest the host magma derivation from a

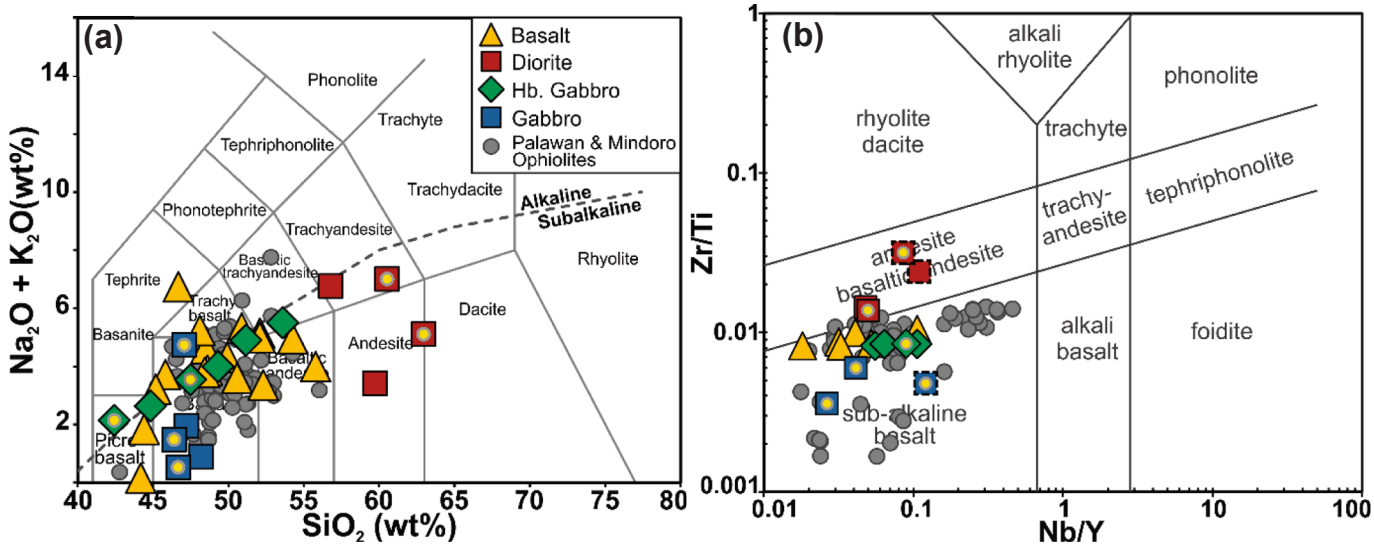

Fig. 7. Plots of (a) total alkalis vs. silica (Le Maitre et al., 1989) and (b) Nb/Y vs. Zr/Ti (Winchester and Floyd, 1977; Pearce, 1996). Dated samples are marked with yellow dots. Mafic magmatic rocks from the Central Palawan and Amnay ophiolites (Yumul et al., 2009; Perez et al., 2013; Yu et al., 2020; Gibaga et al., 2020; Dycoco et al., 2021) are plotted for comparison.

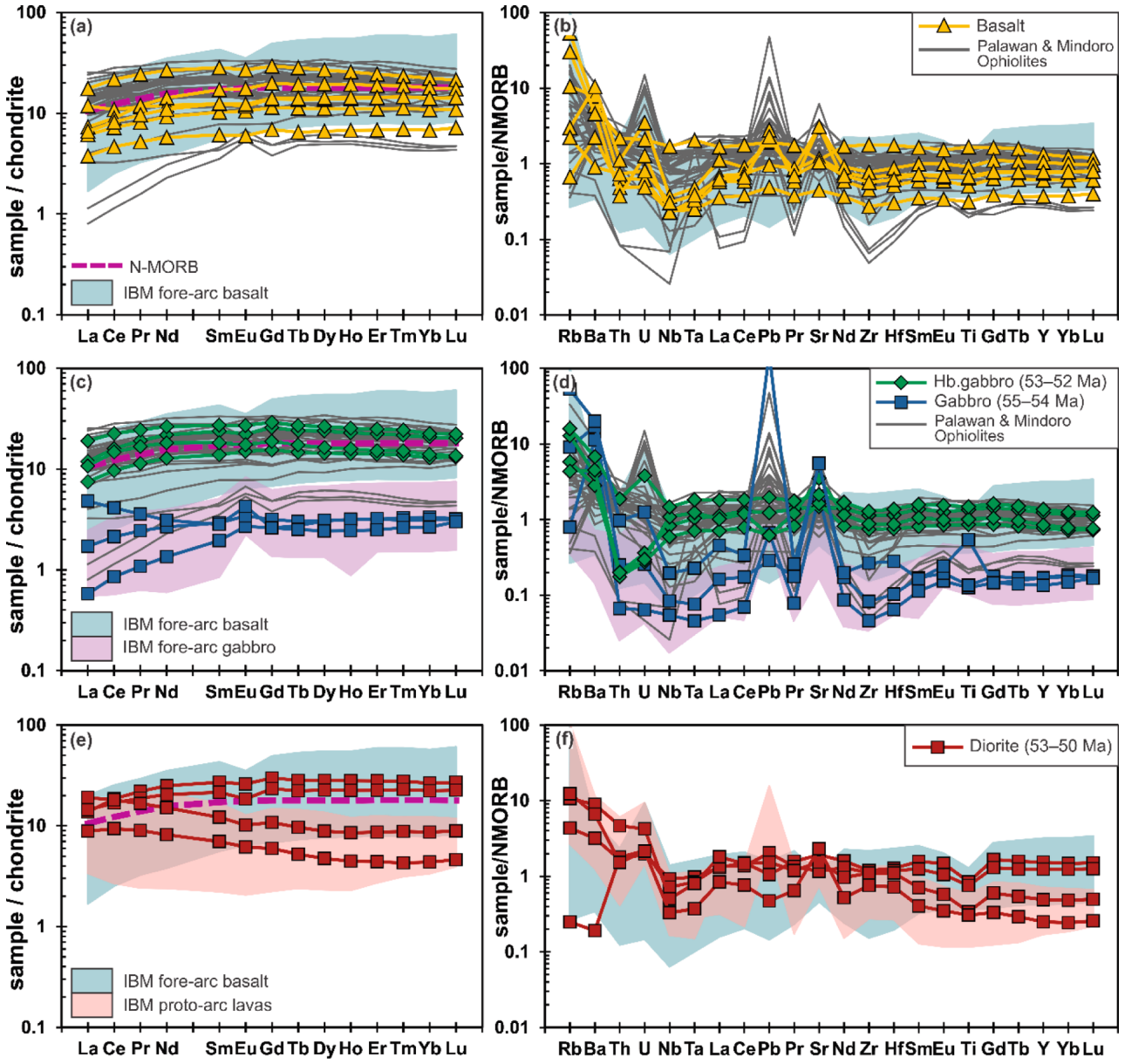

Fig. 8. Chondrite-normalized REE and N-MORB-normalized element patterns of the Banggi Island Ophiolite: (a-b) basalts, (c-d) gabbros and Hb gabbros, and (e-f) diorites. Mafic rocks from the Central Palawan and Amnay ophiolites are also plotted for comparison. N-MORB and chondrite values are from Sun and McDonough (1989). The Izu-Bonin-Mariana (IBM) fore-arc data are compiled from Pearce et al. (1999); Reagan et al. (2010, 2013); Ishizuka et al. (2011); Coulthard (2018); Shervais et al. (2019).

depleted or juvenile mantle source. In the Nb/Yb vs Th/Yb diagram (Fig. 9a), they are plotted in between the mantle array and the oceanic arc lavas, suggesting an addition of the subduction-mobile element Th in the SSZ-type tectonic environment (Pearce et al., 2005). Three samples of hornblende gabbro, however, are plotted far below the mantle array, as a result of strong depletion in Th (Fig. 8d) that appears rare in the literature and ascribed to melting of a depleted mantle wedge fluxed by a subducted serpentinite-derived fluid (Whalen et al., 2003). In the TiO_2 vs MgO tectonic discrimination diagram (Fig. 9b), delineated by Lin et al. (2023) using young magmatic rocks from the SSZ-type Timor ophiolite in the Banda forearc setting, the BIO samples are plotted largely in the initial forearc to arc domains corresponding to the mafic rocks of SSZ-type ophiolites from Central Palawan and Mindoro. Such a correspondence is also observed in the Ti/1000 vs V diagram (Fig. 9c). Combined with the multi-element distribution pattern of the BIO magmatic rocks, which is comparable to that of forearc basalts from the Izu-Bonin-Mariana system (Fig. 8), it is hence concluded that the BIO is an SSZ-type ophiolite that may have originated from the forearc or proto-arc settings at the initial stage of an intra-oceanic subduction.

6.3. *Origin of the BIO – An Eocene SSZ-type ophiolite*

The ophiolites in Sabah have traditionally been claimed as remnants of the PSCS oceanic crust (Omang, 1993; Hutchison, 2005; Hall and Breitfeld, 2017). The PSCS, in the long debate regarding its history, has widely been regarded as a Mesozoic ocean that existed prior to the present-day SCS basin in the region north off Borneo and Palawan (Holloway, 1981; Hinz et al., 1991; Zheng et al., 2019 and refs. therein). Hall and Breitfeld (2017), more specifically, illustrated that the PSCS plate was subducted beneath the region from Sabah to Cagayan during the Eocene and Early Miocene. While the exact age and extent of the PSCS remain uncertain, and beyond the scope of this study, our new

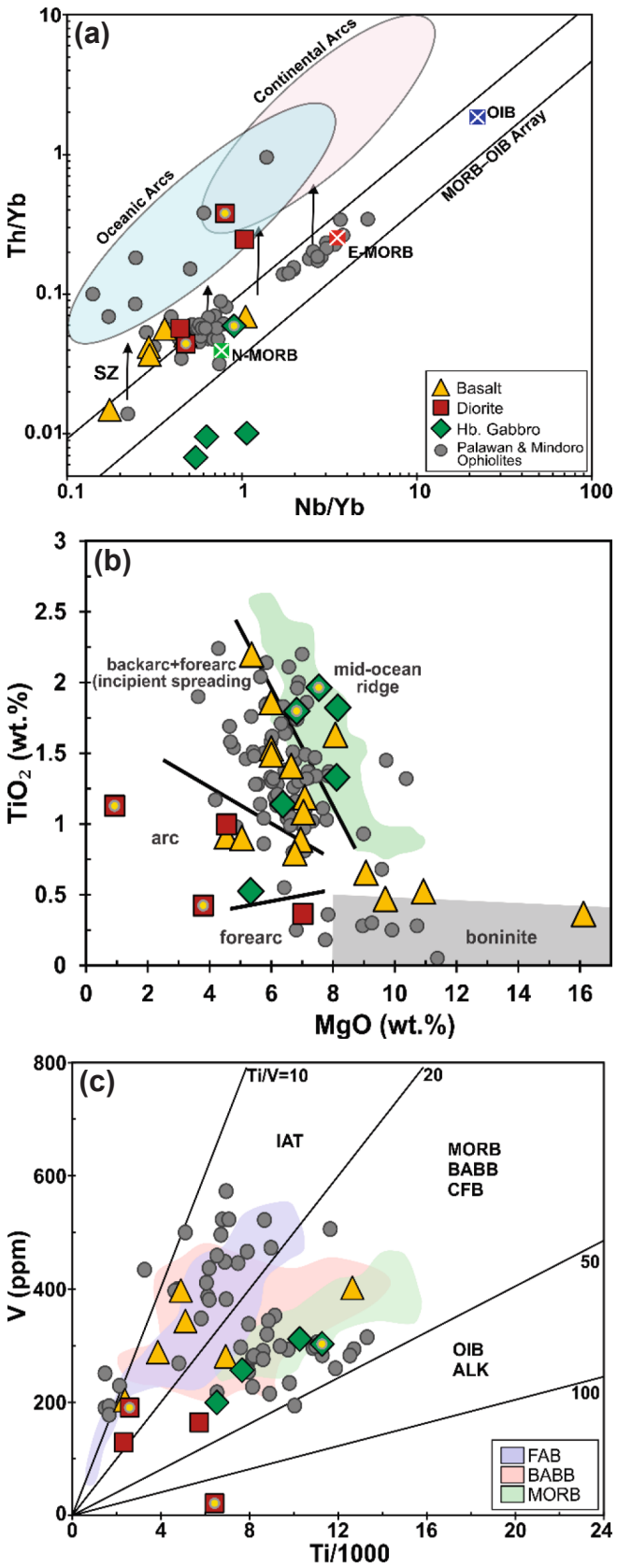

Fig. 9. Geochemical discrimination diagrams of (a) Nb/Yb vs. Th/Yb (Pearce, 2008), (b) MgO vs. TiO_2 (Lin et al., 2023), and (c) Ti/1000 vs. V (Shervais,-vais, 1982).

zircon U-Pb age data obtained from Banggi Island enable us to conclude that the Eocene BIO (~55–50 Ma) is too young to be part of the Mesozoic PSCS oceanic crust.

The BIO magmatic rocks that overall display geochemical characteristics mimicking to forearc basalts from the Izu-Bonin-Mariana system, suggest an SSZ-type petrogenesis related to initiation of an intra-oceanic subduction. Origin of this SSZ-type BIO, therefore, maybe best explained by the upper plate processes associated with the PSCS subduction initiation around Sabah (Fig. 10a), referring to the scenarios described in details from the Izu-Bonin-Mariana forearc system (Stern et al., 2012) or in our more recent study from Timor (Lin et al., 2023). Accordingly, we propose that from the Early Eocene the leading edge of the PSCS plate started being subducted southward beneath the region off Sabah, and thus led to upper-plate spreading and resultant magmatism that gave rise the BIO magmatic rocks in the initial forearc setting (Fig. 10a).

6.4. Broader tectonic interpretations

Our model of the PSCS subduction initiation requires another previously existing but presently absent ocean basin in the upper plate that we call for the East Asian Sea (Wu et al., 2016), with its westernmost part in contact with Borneo (Fig. 10a) and evolved subsequently to form the Celebes Sea (Wu et al., 2016). Records of such a pre-Eocene ocean basin appear preserved elsewhere in northern Sabah, from the Kudat and Marudu Bay ophiolites (i.e., KO and MBO; Fig. 1b), from which N-MORB type gabbros yield zircon U-Pb ages dated at ~ 128–122 Ma (Rezal et al., 2020; 2025; Wang et al., 2023), with Barremian-Cenomanian radiolarian fossils observed in associated sedimentary formations (Basir et al., 1985; Basir and Tongkul, 2013). Rezal et al. (2025) therefore argue whereas the Eocene BIO was formed in a forearc regime at the earliest stage of southward subduction of the PSCS plate, the Early Cretaceous KO and MBO may represent fragments of the overriding East Asian Sea plate involved in this subduction system. Hence, the Cretaceous zircon grains observed in some BIO samples (Table S2) are likely sourced from the upper plate during the initial forearc magmatism (Fig. 10). Such coexistence of Cretaceous vs Paleogene ophiolitic rocks have also been observed from Palawan to Mindoro and Luzon, the western Philippines (Encarnacion et al., 1993; Keenan et al., 2016; Yu et al., 2020; Yumul et al., 2020; Dycoco et al., 2021), despite a variety of complex models proposed by these studies.

We furthermore argue for a progressive eastward migration of the PSCS subduction initiation (Fig. 10b), based on the east-younging trend of the SSZ-type ophiolites from Central Palawan (~40–34 Ma; Keenan et al., 2016; Dycoco et al., 2021) and Amnay, Mindoro (~33–23 Ma; Yu et al., 2020). Bounded in the west by the West Baram Line (Cullen, 2014), the PSCS subduction was ultimately truncated in the eastern end by the northwestward-moving Luzon subduction system in the Early Miocene (Chung et al., 2025), when the latter moved up to its corresponding position (Wu et al., 2016). Continued development of the PSCS southward subduction resulted in a magmatic arc, i.e., the Sabah-Cagayan Arc (Fig. 10b), now exposed as the Cagayan Ridge, which was most active during ~ 40–21 Ma and then terminated by the arc-continent collision owing to arrival of the rifted Eurasian fragments (cf. Hall, 2013). Details about this regional interpretation, nevertheless, will be presented elsewhere in a separate paper in preparation.

6.5. Implication for the Eocene unconformity

The Eocene stratigraphic unconformity (Fig. 2) occurs widely in Sabah and neighbouring areas (e.g., Sarawak, northwestern Borneo and Palawan, western Philippines). However, its cause or even exact stratigraphic position (Jamil et al., 2020) remains debated. The discovery of the Early Eocene (~55–50 Ma) SSZ-type ophiolite from Banggi Island leads us to relate the Eocene unconformity to the subduction initiation of the PSCS plate around Sabah. We hence argue that a major tectonic

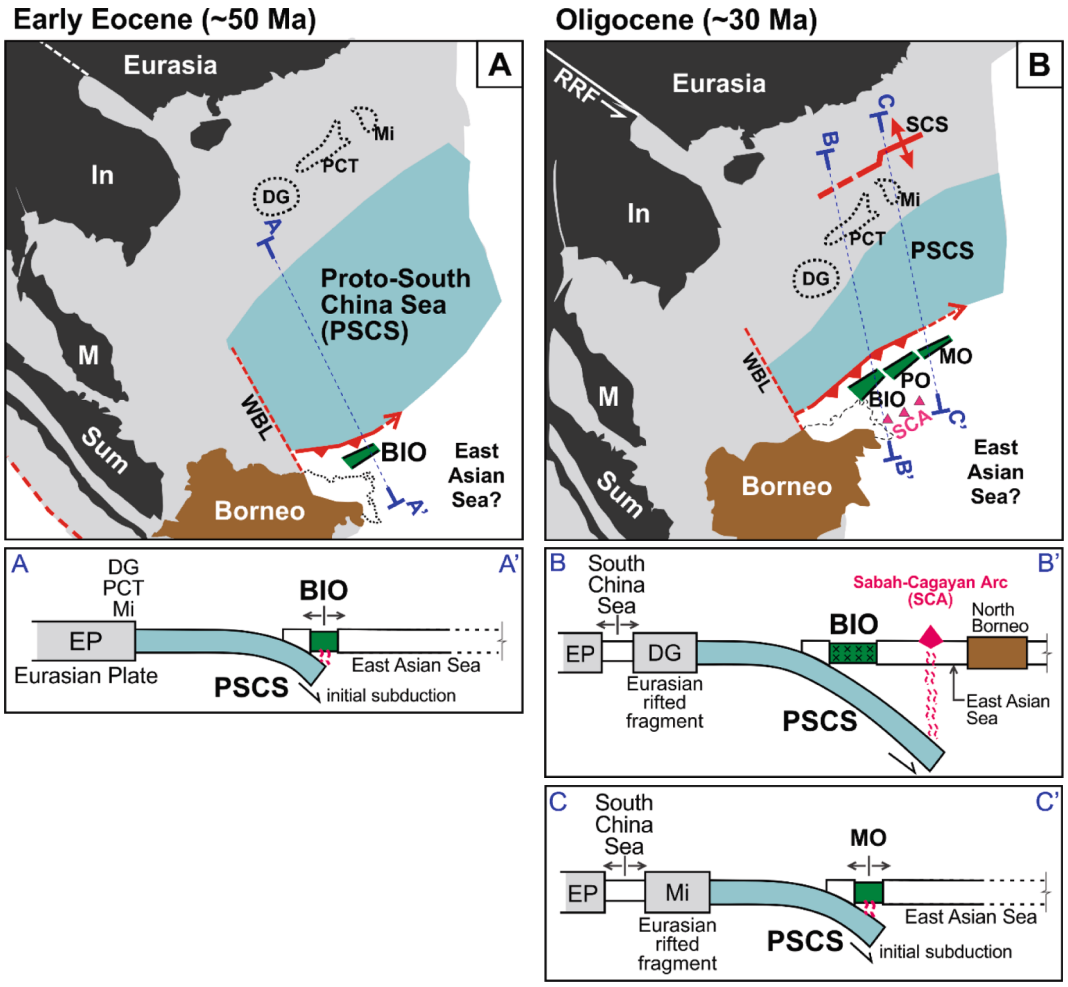

Fig. 10. A plate reconstruction model illustrating (a) formation of the Banggi Island Ophiolite by southward subduction initiation of the PSCS oceanic plate around Sabah, followed by (b) progressive eastward subduction initiation to form the PO and the MO, respectively, in the forearc setting. Abbreviation: In = Indochina; M = Malaya; Sum=Sumatra; SCS=South China Sea; PSCS=Proto-South China Sea; DG = Dangerous Ground (Nansha block); PCT=Palawan Continental Terrain; Mi = Mindoro; BIO = Banggi Island Ophiolite; PO=Central Palawan Ophiolite; MO = Mindoro (Amnay) Ophiolite; RRF = Red River Fault; WBL = West Baram Line. Note that cross-sections are not to scale.

event as such may have accounted for regional uplift and subsequent sedimentary hiatus that gave rise to the Eocene unconformity and related deformations reported from Sabah and elsewhere in northern Borneo (Bénard et al., 1990; Tongkul, 1997; Wang et al., 2016). While the PSCS subduction initiation was responsible for the Eocene unconformity and even the Sarawak Orogeny, its cessation that resulted from the arrival and collision of the micro-continental fragments (Hall, 2013) may have played a key role in causing the Miocene unconformity as well as the Sabah Orogeny (Hutchison et al., 2000; Hutchison, 2005; 2007; Lunt and Madon, 2017).

CRediT authorship contribution statement

Rezal Rahmat: Writing – original draft, Validation, Investigation, Formal analysis, Data curation. **Sun-Lin Chung:** Writing – review & editing, Writing – original draft, Supervision, Investigation, Data curation, Conceptualization. **Azman Abd Ghani:** . **Hao-Yang Lee:** Supervision, Methodology, Data curation. **Yoshiyuki Iizuka:** Methodology, Investigation, Data curation. **Chih-Tung Chen:** Supervision, Investigation. **Long Xiang Quek:** .

Declaration of competing interest

The authors declare that they have no known competing financial interests or personal relationships that could have appeared to influence the work reported in this paper.

Acknowledgements

Rezal Rahmat thanks the Taiwan International Graduate program, Earth System Science at the Academia Sinica for providing fellowship. This study was supported by a series of grants, most recently by the National Science and Technology Council, Taiwan (grant no. 114-2116-M-001-003) and Academic Sinica, Taiwan (grant no. AS-IVA-112-M02) to SLC. We thank Associate Editor Ibrahim Uysal and two anonymous reviewers for their constructive comments that helped improve the quality of this paper. We also thank H. Wang for help with mineral separation, and Chien-Hui Hung, Yi-Ru Hsin, Chiu-Hong Chu and You-Jhen Chen for lab assistance.

Authorship contributions

RR - performing fieldwork, lab analysis, data visualization and writing.

SLC - conceptualization, supervision and writing.

AAG, CTC and LXQ - fieldwork and discussion.

HYL and YI - analytical data acquisition.

All authors contributed ideas to the interpretation of results or

manuscript revisions.

Appendix A. Supplementary data

Supplementary data to this article can be found online at https://doi.org/10.1016/j.jseaes.2025.106919.

Data availability

Data will be made available on request.

References

Aitchison, J.C., 1994. Early Cretaceous (pre-Albian) radiolarians from blocks in Ayer Complex melange, eastern Sabah, Malaysia, with comments on their regional tectonic significance and the origins of enveloping melanges. J. Southeast Asian Earth Sci. 9, 255–262.

Andersen, T., 2002. Correction of common lead in U–Pb analyses that do not report ^{204}Pb. Chem. Geol. 192 (1–2), 59–79.

Anonymous., 1972. Penrose field conference on ophiolites. Geotimes 17 (12), 24–25.

Basir, J., Sanudin, T., Abdul Rahim, S., 1985. Lower Cretaceous radiolaria from the Chert-Spilite Formation, Kudat, Sabah. Warta Geologi 11, 161–162.

Basir, J., 1992. Significance of radiolarian cherts from the Chert-Spilite Formation, Telupid, Sabah. Geological Society of Malaysia Bulletin 31, 67–83.

Basir, J., Tongkul, F., 2013. Cretaceous radiolarians from Baliojong ophiolite sequence, Sabah. Malaysia. Journal of Asian Earth Sciences. 76, 258–265.

Bénard, F., Muller, C., Letouzey, J., Rangin, C., Tahir, S., 1990. Evidence of multiphase deformation in the Rajang-Crocker Range (northern Borneo) from Landsat imagery interpretation: Geodynamic implications. Tectonophysics 183 (1–4), 321–339.

Briais, A., Patriat, P., Tapponnier, P., 1993. Updated interpretation of magnetic anomalies and seafloor spreading stages in the South China Sea: Implications for the Tertiary tectonics of Southeast Asia. J. Geophys. Res. 98, 6299–6328.

Burton-Johnson, A., Macpherson, C.G., Millar, I.L., Whitehouse, M.J., Ottley, C.J., Nowell, G.M., 2020. A Triassic to Jurassic arc in north Borneo: Geochronology, geochemistry, and genesis of the Segama Valley Felsic Intrusions and the Sabah ophiolite. Gondw. Res. 84, 229–244.

Chen, Y., Niu, Y., Shen, F., Gao, Y., Wang, X., 2020. New U–Pb zircon age and petrogenesis of the plagiogranite, Troodos ophiolite. Cyprus. Lithos 362, 105472.

Chien, Y. H., Wang, K. L., Chung, S. L., Ghani, A. A., Iizuka, Y., Li, X. H., and Lee, H. Y., 2019. Age and genesis of Sabah Ophiolite complexes in NE Borneo. In *Goldschmidt Abstracts*, p. 598.

Chiu, H.-Y., Chung, S.-L., Zarrinkoub, M.H., Mohammadi, S.S., Khatib, M.M., Iizuka, Y., 2013. Zircon U–Pb age constraints from Iran on the magmatic evolution related to Neotethyan subduction and Zagros orogeny. Lithos 162–163, 70–87.

Chung, S.-L., Lin, Y.-C., Rezal, R., Ghani, A., Lee, H.-Y., 2025. An ophiolite perspective on Asia orogeny: Propagating subduction initiation from Sabah to Taiwan. Abstract to The Geochemical Society of Japan, Annual Meeting.

Coulthard Jr, D.A., 2018. *Subduction initiation and igneous petrogenesis: characterizing melt generation at a new convergent boundary through the geochemical analysis of volcanic glass*. University of Iowa, p. 63p. Master's Thesis (unpublished.

Cullen, A., 2014. Reprint of: nature and significance of the West Baram and Tinjar Lines, NW Borneo. Mar. Pet. Geol. 58, 674–686.

Cullen, A., Burton-Johnson, A., 2021. [Comment] New zircon radiometric U-Pb ages and Lu-Hf isotopic data from the ultramafic-mafic sequences of Ranau and Telupid (Sabah, eastern Malaysia): Time to reconsider the geological evolution of Southeast Asia? Geology 49 (11), 541.

Dycoco, J.M.A., Payot, B.D., Valera, G.T.V., Labis, F.A.C., Pasco, J.A., Perez, A.D., Tani, K., 2021. Juxtaposition of Cenozoic and Mesozoic ophiolites in Palawan Island, Philippines: New insights on the evolution of the Proto-South China Sea. Tectonophysics 819, 229085.

Encarnacion, J.P., Mukasa, S.B., Obille, E.C., 1993. Zircon U-Pb geochronology of the Zambales and Angat ophiolites, Luzon, Philippines: evidence for an Eocene arc backarc pair. J. Geophys. Res. 98 19991e20004.

Fitch, R. H., 1955. The geology and mineral resources of part of the Segama Valley and Darvel Bay area. Colony of North Borneo. *British Borneo Geological Survey Memoir* **4**.

Gibaga, C.R.L., Arcilla, C.A., Hoang, N., 2020. Volcanic rocks from the Central and Southern Palawan Ophiolites, Philippines: Tectonic and mantle heterogeneity constraints. Journal of Asian Earth Sciences: X 4, 100038.

Graves, J.E., Hutchison, C.S., Bergman, S.C., Swauger, D.A., 2000. Age and MORB geochemistry of the Sabah Ophiolite basement. Geological Society of Malaysia Bulletin 44, 151–158.

Hall, R., 2012. Late Jurassic–Cenozoic reconstructions of the Indonesian region and the Indian Ocean. Tectonophysics 570, 1–41.

Hall, R., 2013. Contraction and extension in northern Borneo driven by subduction rollback. J. Asian Earth Sci. 76, 399–411.

Hall, R., Spakman, W., 2015. Mantle structure and tectonic history of SE Asia. Tectonophysics 658, 14–45.

Hall, R., Breitfeld, H.T., 2017. Nature and demise of the Proto-South China Sea. Geological Society of Malaysia Bulletin 63, 61–76.

Hinz, K., Block, M., Kudrass, H.R., Meyer, H., 1991. Structural elements of the Sulu Sea, Phillipines. Geologisches Jahrbuch, Reihe A 127, 483–506.

Holloway, N.H., 1981. The North Palawan block, Philippines: its relation to the Asian mainland and its role in the evolution of the South China Sea. Geological Society of Malaysia Bulletin 14, 19–58.

Hsin, Y.J., 2018. *Age and geochemical characteristics of Neogene volcanic rocks from SE Sabah, Borneo*. National Taiwan University, (in Chinese with English abstract). Master Thesis (unpublished.

Hutchison, C.S., 1975. Ophiolite in southeast Asia. Geol. Soc. Am. Bull. 86 (6), 797–806.

Hutchison, C.S., 1996. The 'Rajang accretionary prism' and 'Lupar Line' problem of Borneo. In: Hall, R., Blundell, D. (Eds.), Tectonic Evolution of Southeast Asia, 106. Geological Society of London Special Publication, pp. 247–261.

Hutchison, C.S., Bergman, S.C., Swauger, D.A., Graves, J.E., 2000. A Miocene collisional belt in north Borneo: uplift mechanism and isostatic adjustment quantified by thermochronology. J. Geol. Soc. London 157 (4), 783–793.

Hutchison, C.S., 2005. *Geology of North-West Borneo (Sarawak, Brunei and Sabah)*. Elsevier, Amsterdam.

Hutchison, C.S., 2007. *Geological Evolution of South-East Asia*, 2nd edn. Geological Society of Malaysia, Kuala Lumpur, Malaysia.

Ishizuka, O., Tani, K., Reagan, M.K., Kanayama, K., Umino, S., Harigane, Y., Sakamoto, I., Miyajima, Y., Yussa, M., Dunkley, D.J., 2011. The timescales of subduction initiation and subsequent evolution of an oceanic island arc. Earth Planet. Sci. Lett. 306 (3–4), 229–240.

Jackson, S.E., Pearson, N.J., Griffin, W.L., Belousova, E.A., 2004. The application of laser ablation-inductively coupled plasma-mass spectrometry to in situ U–Pb zircon geochronology. Chem. Geol. 211 (1–2), 47–69.

Jamil, M., Abd Rahman, A.H., Siddiqui, N.A., Ibrahim, N.A., Ahmed, N., 2020. A contemporary review of sedimentological and stratigraphic framework of the Late Paleogene deep marine sedimentary successions of West Sabah, North-West Borneo. Bulletin of the Geological Society of Malaysia 69 (1), 53–65.

Junaidi, A., Basir, J., 2012. Aptian to Turonian Radiolaria from Darvel Bay Ophiolite Complex, Kunak, Sabah. Geological Society of Malaysia Bulletin 58, 89–96.

Junaidi, A., Basir, J., 2013. Aptian to Turonian Radiolarians from Chert Blocks in the Kuamut Melange, Sabah. Malaysia. Sains Malaysiana 42 (5), 561–570.

Keenan, T.E., Encarnación, J., Buchwaldt, R., Fernandez, D., Mattinson, J., Rasoazanamparany, C., Luetkemeyer, P.B., 2016. Rapid conversion of an oceanic spreading center to a subduction zone inferred from high-precision geochronology. PNAS 113 (47), E7359–E7366.

Kirk, H.J.C., 1968. *The Igneous Rocks of Sarawak and Sabah*. Geological Survey, Borneo Region, Malaysia, Bulletin, p. 5.

Le Maitre, R.W., Bateman, P., Dudek, A., Keller, J., Lameyre, J., Le Bas, M.J., Sabinem, P. A., Schmid, R., Sorensen, H., Streckeisen, A., Woolley, A.R., Zanettin, B., 1989. *A classification of igneous rocks and a glossary of terms*. Blackwell Scientific, Oxford, pp. 1–236.

Leong, K. M., 1974. *The geology and mineral resources of the Upper Segama Valley and Darvel Bay area, Sabah, Malaysia*. Geological Survey of Malaysia, Memoir **4**, (revised).

Leong, K.M., 1977. New ages from radiolarian cherts of the Chert–Spilite Formation. Geological Society of Malaysia Bulletin 8, 109–111.

Lin, Y.C., Chung, S.L., Maruyama, S., Kadarusman, A., Lee, H.Y., 2023. The ephemeral history of Earth's youngest supra-subduction zone type ophiolite from Timor. Commun. Earth Environ. 4 (1), 308.

Lunt, P., Madon, M., 2017. Onshore to offshore correlation of northern Borneo; a regional perspective. Geological Society of Malaysia Bulletin 64, 101–122.

Newton-Smith, J., 1967. *Bidu-Bidu Hills, area, Sabah*. East Malaysia, Geological Survey of Malaysia, Kuching, Report, p. 4.

Omang, S., A. K., Wan Azmona Wan Mohamed, Sanudin T. and Sahibin, A. R, 1992. The Darvel Bay Ophiolite Complex, SE Sabah. Malaysia-Preliminary interpretation. Warta Geologi 18 (3), 81–88.

Omang, S., A. k.,, 1993. *Petrology, Geochemistry and Structural Geology of the Darvel Bay Ophiolite, Sabah, Malaysia*. University of London, p. 446p. Ph.D. Thesis (unpublished.

Omang, S., A. K., Majeed, M. F. and Sanudin T, 1994. The Kudat Ophiolite Complex, Northern Sabah. Malaysia-Field description and disscusion. Warta Geologi 20 (5), 337–345.

Omang, S., A. K., and Barber, A. J., 1996. Origin and tectonic significance of the metamorphic rocks associated with the Darvel Bay ophiolite, Sabah, Malaysia. In: Hall, R., Blundell, D. (Eds.), Tectonic evolution of Southeast Asia, 106. Geological Society of London Special Publication, pp. 263–279.

Pearce, J.A., 1996. A user's guide to basaltic discrimination diagrams, *in* Wyman, D. A., ed., *Trace Element Geochemistry of Volcanic Rocks: Applications for Massive Sulphide Exploration, Geological Association of Canada Short Course*. Notes 12, 79–113.

Pearce, J.A., Kempton, P.D., Nowell, G.M., Noble, S.R., 1999. Hf-Nd element and isotope perspective on the nature and provenance of mantle and subduction components in Western Pacific arc-basin systems. J. Petrol. 40 (11), 1579–1611.

Pearce, J.A., Stern, R.J., Bloomer, S.H., Fryer, P., 2005. Geochemical mapping of the Mariana arc-basin system: Implications for the nature and distribution of subduction components. Geochem. Geophys. Geosyst. 6 (7).

Pearce, J.A., 2008. Geochemical fingerprinting of oceanic basalts with applications to ophiolite classification and the search for Archean oceanic crust. Lithos 100, 14–48.

Perez, A.C., Faustino-Eslava, D.V., Yumul Jr, G.P., Dimalanta, C.B., Tamayo Jr, R.A., Yang, T.F., Zhou, M.F., 2013. Enriched and depleted characters of the Amnay Ophiolite upper crustal section and the regionally heterogeneous nature of the South China Sea mantle. J. Asian Earth Sci. 65, 107–117.

Rangin, C., Bellon, H., Benard, P., Letouzey, J., Muller, C., Sanudin, T., 1990. Neogene arc-continent collision in Sabah, Northern Borneo (Malaysia). Tectonophysics 183, 305–319.

Rangin, C., Spakman, W., Pubellier, M., Bijwaard, H., 1999. Tomographic and geological constraints on subduction along the eastern Sundaland continental margin (South-East Asia). Bulletin de la Société Géologique de France 170 (6), 775–788.

Razak, Y. A., 2015. *Geological Map of Sabah, 1:500,000*, 4th Edition. Minerals and Geoscience Malaysia.

Reagan, M.K., Ishizuka, O., Stern, R.J., Kelley, K.A., Ohara, Y., Blichert-Toft, J., Bloomer, S.H., Cash, J., Fryer, P., Hanan, B.B., Hickey-Vargas, R., Ishii, T., Kimura, J.-I., Peate, D.W., Rowe, M.C., Woods, M., 2010. Fore-arc basalts and subduction initiation in the Izu-Bonin-Mariana system. Geochem. Geophys. Geosyst. 11 (3).

Reagan, M.K., McClelland, W.C., Girard, G., Goff, K.R., Peate, D.W., Ohara, Y., Stern, R. J., 2013. The geology of the southern Mariana fore-arc crust: Implications for the scale of Eocene volcanism in the western Pacific. Earth Planet. Sci. Lett. 380, 41–51.

Rezal, R., 2016. *Petrology of The Marudu Bay Ophiolite Complex (MBOC)*. Master Thesis (unpublished), Universiti Malaysia Sabah, 446p (in. Malay with English abstract), Northern Sabah, Malaysia.

Rezal, R., Chung, S.L., Ghani, A.A., Lee, H.Y., Iizuka, Y., 2020. Zircon U–Pb Ages and Geochemical Characteristics of Mafic Rocks from Northern Sabah Ophiolite (Borneo). In Goldschmidt Abstracts, Malaysia, p. 2020.

Rezal, R., Chung, S. L., Chen, C. T., Ghani, A. A., Lee, H. Y., Iizuka, Y., & Quek, L. X. 2025. Juxtaposed Cretaceous and Eocene Ophiolites in Northern Sabah (Borneo), Malaysia: Insights from U-Pb Geochronology, Geochemistry, and Tectonic Significance. In *Malaysia National Geoscience Conference (NGC 2025) Abstracts*.

Rollinson, H., 2009. New models for the genesis of plagiogranites in the Oman ophiolite. Lithos 112 (3–4), 603–614.

Sanudin, T., Baba, M., 2007. *Pengenalan Kepada Stratigrafi*. Universiti Malaysia Sabah, Kota Kinabalu, Sabah.

Shervais, J.W., 1982. Ti–V plots and the petrogenesis of modern and ophiolitic lavas. Earth Planet. Sci. Lett. 59 (1), 101–118.

Shervais, J.W., Reagan, M., Haugen, E., Almeev, R.R., Pearce, J.A., Prytulak, J., Ryan, J. G., Whattam, S.A., Godard, M., Chapman, T., Li, H., Kurz, W., Nelson, W.R., Heaton, D., Kirchenbaur, M., Shimizu, K., Sakuyama, T., Li, Y., Vetter, S.K., 2019. Magmatic response to subduction initiation: Part 1. Fore-arc basalts of the Izu-Bonin arc from IODP Expedition 352. Geochem. Geophys. Geosyst. 20 (1), 314–338.

Sibuet, J.-C., Yeh, Y.-C., Lee, C.-S., 2016. Geodynamics of the South China Sea. Tectonophysics 692, 98–119. https://doi.org/10.1016/j.tecto.2016.02.022.

Stephens, E. A., 1956. The geology and mineral resources of the Kota Belud and Kudat area North Borneo. Geological Survey Department, British Territories in Borneo, Memoir 5.

Stern, R.J., Reagan, M., Ishizuka, O., Ohara, Y., Whattam, S., 2012. To understand subduction initiation, study forearc crust: To understand forearc crust, study ophiolites. Lithosphere 4 (6), 469–483.

Sun, S.-S., McDonough, W.F., 1989. Chemical and isotopic systematics of oceanic basalts: implications for mantle composition and processes. Geol. Soc. Lond. Spec. Publ. 42 (1), 313–345.

Swauger, D., Bergman, S.C., Graves, J., Hutchison, C.S., Surat, T., Morillo, A.P., Benavidez, J.J., Pagado, E.S., 1995. *Tertiary Strati graphic. Tectonic, and Thermal History of Sabah, Malaysia: Results of a 1994. Ten Day Reconnaissance Field Study and Laboratory Analyses*. ARCO International Oil and Gas Company, ARCO Exploration and Production Technology.

Tian, Z., Gao, Y., Wang, P., Tang, H., 2024. Formation and Tectonic Evolution of Ophiolites in the Sabah Area (Borneo, SE Asia). Minerals 14 (11), 1078.

Tjia, H.D., 1988. Accretion tectonics in Sabah: Kinabalu Suture and East Sabah accreated terrace. Geological Society of Malaysia Bulletin 22, 237–1221.

Tongkul, F., 1995. The Paleogene basins of Sabah, East Malaysia. Geological Society of Malaysia Bulletin 37, 301–308.

Tongkul, F., 1997. Polyphase deformation in the Telupid area, Sabah. Malaysia. Journal of Asian Earth Sciences 15 (2–3), 175–183.

Tsai, C.H., Shyu, J.B.H., Chung, S.L., Ramos, N.T., Lee, H.Y., 2019. Detrital zircon record from major rivers of Luzon Island: implications for Cenozoic continental growth in SE Asia. J. Geol. Soc. London 176 (4), 727–735.

Tsikouras, B., Lai, C.K., Ifandi, E., Teo, C.H., Xia, X.P., 2021. New zircon radiometric U-Pb ages and Lu-Hf isotopic data from the ultramafic-mafic sequences of Ranau and Telupid (Sabah, eastern Malaysia): Time to reconsider the geological evolution of Southeast Asia? Geology 49 (7), 789–793.

van de Lagemaat, S.H., Cao, L., Asis, J., Advokaat, E.L., Mason, P.R., Dekkers, M.J., van Hinsbergen, D.J., 2024. Causes of Cretaceous subduction termination below South China and Borneo: Was the Proto-South China Sea underlain by an oceanic plateau? Geosci. Front. 15 (2), 101752.

Wang, P.C., Li, S.Z., Guo, L.L., Jiang, S.H., Somerville, I.D., Zhao, S.J., Zhu, B.D., Chen, J., Dai, L.M., Suo, Y.H., Han, B., 2016. Mesozoic and Cenozoic accretionary orogenic processes in Borneo and their mechanisms. Geol. J. 51, 464–489.

Wang, Y., Qian, X., Asis, J.B., Cawood, P.A., Wu, S., Zhang, Y., Feng, Q., Lu, X., 2023. "Where, when and why" for the arc-trench gap from Mesozoic Paleo-Pacific subduction zone: Sabah Triassic-Cretaceous igneous records in East Borneo. Gondw. Res. 117, 117–138.

Whalen, J.B., Percival, J.A., McNicoll, V.J., Longstaffe, F.J., 2003. Intra-oceanic production of continental crust in a Th-depleted ca. 3.0 Ga arc complex, western Superior Province, Canada. Contrib. Miner. Petrol. 146 (1), 78–99.

Wilson, R. A. M., 1961. The geology and mineral resources of the Banggi Island and Sugut River area, North Borneo. Geological Survey Department, British Territories in Borneo, Memoir 15.

Winchester, J.A., Floyd, P.A., 1977. Geochemical discrimination of different magma series and their differentiation products using immobile elements. Chem. Geol. 20, 325–343.

Wu, J., Suppe, J., Lu, R., Kanda, R., 2016. Philippine Sea and East Asian plate tectonics since 52 Ma constrained by new subducted slab reconstruction methods. J. Geophys. Res. Solid Earth 121 (6), 4670–4741.

Yu, M., Dilek, Y., Yumul, G.P., Yan, Y., Dimalanta, C.B., Huang, C.Y., 2020. Slab-controlled elemental–isotopic enrichments during subduction initiation magmatism and variations in forearc chemostratigraphy. Earth Planet. Sci. Lett. 538, 116217.

Yumul Jr, G.P., Jumawan, F.T., Dimalanta, C.B., 2009. Geology, geochemistry and chromite mineralization potential of the Amnay Ophiolitic Complex, Mindoro. Philippines. Resource geology 59 (3), 263–281.

Yumul, G.P., Dimalanta, C.B., Gabo-Ratio, J.A.S., Queaño, K.L., Armada, L.T., Padrones, J.T., Faustino-Eslava, D.V., Payot, B.D., Marquez, E.J., 2020. Mesozoic rock suites along western Philippines: Exposed Proto-South China Sea fragments? Journal of Asian Earth Sciences: X 4, 100031.

Zahirovic, S., Seton, M., Müller, R.D., 2014. The cretaceous and Cenozoic tectonic evolution of Southeast Asia. Solid Earth 5 (1), 227–273.

Zhang, X.C., Li, H.Y., Yao, Y., Chen, W.H., 2025. On-land evidence for subduction of the proto-South China Sea beneath northern Borneo and tectonic reconstruction of Southeast Asia during the early Permian-Oligocene. Geol. Soc. Am. Bull. 137 (5–6), 2632–2646. https://doi.org/10.1130/B37901.1.

Zhao, Z., Tang, W., Liu, S., Tang, H., Wang, P., Tian, Z., 2024. U-Pb zircon ages and petrogeochemistry and tectonic implications of gabbro and granite in southwest Lahad Datu area of Sabah. Malaysia. Acta Oceanologica Sinica 43 (2), 94–110.

Zheng, H., Sun, X., Wang, P., Chen, W., Yue, J., 2019. Mesozoic tectonic evolution of the Proto-South China Sea: A perspective from radiolarian paleobiogeography. J. Asian Earth Sci. 179, 37–55.